European Journal of Inorganic Chemistry

EurJIC
European Journal of Inorganic Chemistry

Chemistry Europe
European Chemical Societies Publishing

RESEARCH ARTICLE OPEN ACCESS

Influence of Rosmarinic Acid on Zinc(II)–Amyloid Beta Coordination

Arian Kola | Daniela Valensin

Department of Biotechnology, Chemistry and Pharmacy, University of Siena, Siena, Italy

Correspondence: Daniela Valensin (daniela.valensin@unisi.it)

Received: 1 July 2025 | **Revised:** 31 October 2025 | **Accepted:** 5 November 2025

Keywords: amyloid-β | metal-complex | NMR | polyphenols | rosmarinic acid | ternary association | zn(II)

ABSTRACT

Natural polyphenols such as rosmarinic acid (RA) are gaining attention for their antioxidant, anti-inflammatory, and neuroprotective properties, attributed in part to their ability to chelate redox-active metals. While RA's interactions with Cu(II) have been linked to modulation of amyloid beta (Aβ) aggregation and redox cycling, its coordination with Zn(II)—a key player in Aβ aggregation but redox-inert—remains poorly understood. Given that Zn(II) stabilizes toxic Aβ oligomers and is abundant in amyloid plaques, clarifying whether RA can modulate Zn(II)-Aβ interactions is of high interest. Here, we systematically investigated RA's coordination behavior toward Zn(II) under physiologically relevant conditions, both alone and in the presence of Aβ. Using NMR and UV–vis spectroscopy, we characterized RA-Zn(II) complex formation and explored how RA influences Zn(II)-mediated Aβ associations. These findings provide new insights into the molecular basis of RA's potential neuroprotective effects and underscore the importance of targeting metal–amyloid interactions in Alzheimer's disease.

1 | Introduction

Natural polyphenols, such as rosmarinic acid (RA), have attracted increasing interest for their potential to interfere with amyloidogenic protein interactions [1–9], mitigate oxidative stress [1, 10–12], and prevent neurotoxicity [1, 12–16]. These compounds, widely distributed in medicinal herbs and dietary sources, are characterized by the presence of multiple hydroxyl groups, which enable them to chelate redox-active metal ions such as copper and iron [17, 18]. This metal-chelating ability is particularly relevant in neurodegenerative diseases, where the aberrant accumulation of transition metals contributes to protein misfolding, aggregation, and the generation of reactive oxygen species (ROS). In addition to their antioxidant properties, polyphenols like RA exhibit anti-inflammatory activity, modulate intracellular signaling pathways, and have been shown to preserve mitochondrial function and neuronal viability in vitro and in vivo models [19].

RA is a natural polyphenolic compound widely distributed in Lamiaceae herbs, such as rosemary (*Rosmarinus officinalis*), perilla (*Perilla frutescens*), and lemon balm (*Melissa officinalis*). Structurally, RA is an ester of caffeic acid and 3,4-dihydroxyphenyllactic acid, containing two catechol moieties that confer potent antioxidant and metal-chelating properties. These functionalities enable RA and related polyphenols to coordinate various biologically relevant metal ions, including copper(II), iron(III), and zinc(II), through electron pair donation from phenolic hydroxyl groups [5, 17, 18, 20–26].

Amyloid beta (Aβ) is a peptide derived from the proteolytic cleavage of the amyloid precursor protein (APP) [27]. The self-assembly of Aβ into oligomers and fibrils is a hallmark of Alzheimer's disease (AD) [28]. Among the various molecular factors implicated in Aβ aggregation and toxicity, metal ions such as zinc(II) play a pivotal role. Zn(II) is highly abundant in the synaptic cleft and is known to modulate Aβ aggregation by stabilizing oligomeric species and promoting plaque formation [29–32]. It also promotes aggregation into amorphous, nonfibrillar assemblies and inhibits fibrillogenesis under certain conditions [33]. Although Zn(II) is not redox-active under physiological

conditions, its dysregulation contributes to oxidative stress and neuronal dysfunction through indirect mechanisms [34–36]. While Zn(II) does not participate in redox cycling like Fe(III)/Fe(II) or Cu(II)/Cu(I), it can influence oxidative stress by modulating signaling pathways and protein conformational states. Dysregulation of Zn(II) homeostasis has been associated with neurodegenerative diseases, particularly AD, where it is found enriched in amyloid plaques [37, 38].

Zn(II) binds to Aβ via histidine residues, primarily His6, His13, and His14, forming coordination complexes that affect peptide conformation and aggregation kinetics. The binding stoichiometry and coordination geometry are influenced by pH, Zn(II) concentration, and the presence of competing ligands [37, 39–42].

RA has demonstrated promising capabilities in modulating metal–amyloid-β (Aβ) interactions, particularly in the presence of Cu(II), where it is involved in a ternary complex with the peptide, thereby influencing redox cycling and aggregation behavior [5].

Despite this, the coordination chemistry of RA with Zn(II)—a redox-inactive yet aggregation-relevant metal ion—remains poorly characterized, especially within the context of Aβ binding. From a structural standpoint, Zn(II) preferentially adopts tetrahedral coordination geometries and binds ligands bearing oxygen or nitrogen donor atoms. The catechol moiety of RA, containing two adjacent hydroxyl groups, may serve as a bidentate ligand capable of forming five-membered chelate rings with Zn(II), potentially stabilizing distinct coordination species depending on pH, ionic strength, and metal-to-ligand stoichiometry. Given the ability of RA to chelate divalent metal ions, it is plausible that RA could modulate Zn(II)-induced Aβ aggregation pathways, either by competing for Zn(II) binding, altering the peptide's coordination environment, or affecting the physicochemical features of the aggregation process itself. Clarifying these interactions is essential for understanding the molecular underpinnings of RA's neuroprotective activity.

To address this, we systematically investigated the coordination behavior of RA toward Zn(II) under physiologically relevant conditions, both in the absence and in the presence of the Aβ peptide. UV–vis and NMR techniques were employed to define the coordination modes of RA with Zn(II) and evaluate the influence of RA on Zn(II)-Aβ interactions.

2 | Results and Discussion

To investigate the coordination behavior of RA with Zn(II) under physiologically relevant conditions, we combined ^{1}H NMR and UV–vis spectroscopy at near-neutral pH using different buffer systems (phosphate, tris(hydroxymethyl)aminomethane (TRIS), and 4-(2-hydroxyethyl)-1-piperazineethanesulfonic acid (HEPES). The metal titrations carried out in phosphate buffer showed markedly weak effects. In particular, the NMR spectra of RA recorded at increasing Zn(II) concentrations, showed progressive but small chemical shift variations mainly in the aromatic region, affecting protons H2, H5, H6, and H8 of the caffeic acid moiety. The maximum shift (~0.02 ppm for H5) indicated a weak and reversible interaction in fast exchange, without signal broadening or aggregation (Figure S1). Similarly, UV–vis titrations of RA revealed the emergence of a weak shoulder near 370 nm upon Zn(II) addition (Figure S2). The shoulder intensity increased gradually up to ~0.75 equivalents, accompanied by a slight red shift and hyperchromic effect, suggesting formation of a labile RA–Zn(II) complex. The spectral changes observed by UV–vis were consistent with the weak interaction detected by NMR.

To assess whether the phosphate buffer system could influence the RA–Zn(II) interaction, UV–vis spectroscopic analyses were also performed using two different buffering agents: TRIS and HEPES. The titration profiles obtained upon progressive addition of Zn(II) showed consistent spectral variations in the characteristic absorption bands of RA. In both systems, Zn(II) addition induced the gradual appearance of a new absorption band at 375 nm, whose intensity increased and eventually reached a plateau at higher metal concentrations, indicating the formation of a stable RA–Zn(II) complex (Figure 1). The emergence of this band at 375 nm is consistent with the deprotonation of the catechol groups and supports the coordination of Zn(II) to RA [43, 44]. In contrast, when the same experiment was performed in phosphate buffer, the spectroscopic response differed markedly (Figure S2). Only minor or irregular absorbance changes were detected, and no distinct complex-related band developed. This result underscores the strong competitive effect of phosphate ions, which form Zn–phosphate species that effectively sequester Zn(II), thereby preventing its coordination to RA.

The titration data shown in Figure 1 were fitted using a 1:1 binding model according to the equation $A = A_{max}*(K_{app}\ [M]/(1 + K_{app}\ [M]))$, where A represents the change in absorbance at 375 nm, A_{max} is the limiting absorbance at saturation,

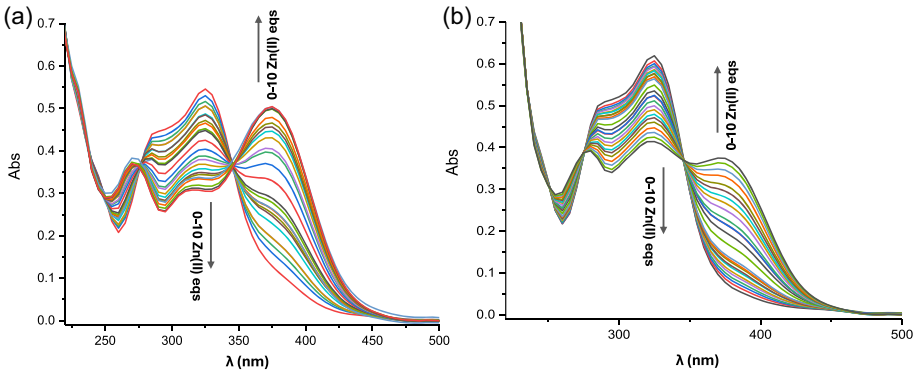

FIGURE 1 | UV–vis spectra of RA 50 μM in the absence and in the presence of increasing Zn(II) ratios (from 0.1–10) in (A) TRIS 15 mM, pH 7.5 and (B) HEPES 15 mM, pH 7.2.

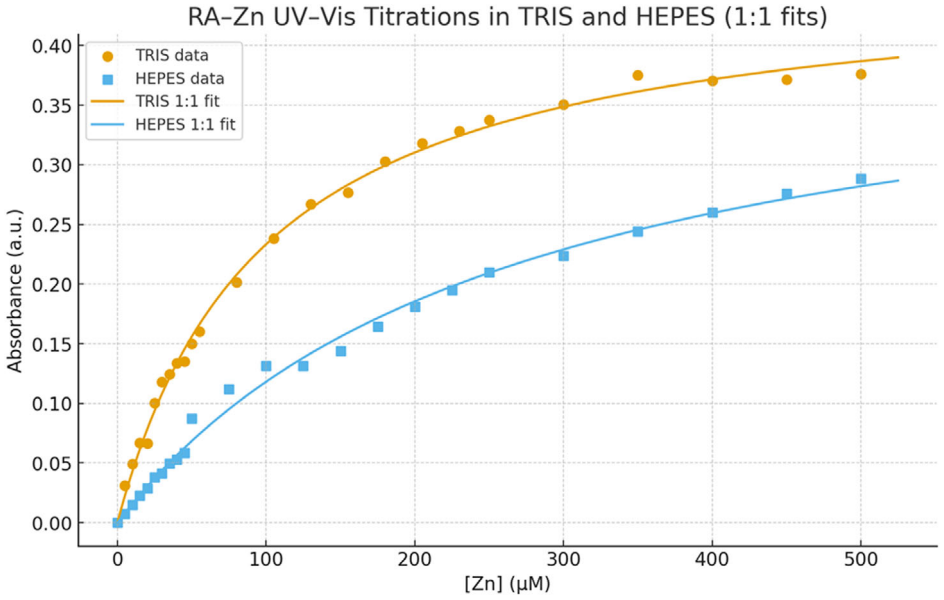

FIGURE 2 | UV–vis titrations of RA 50 μM with Zn(II) in TRIS (orange circle) and HEPES (blue square) buffers. Absorbance values at 375 nm are plotted as a function of total Zn(II) concentration. Data points correspond to experimental titrations, while solid lines represent the best fits obtained assuming a 1:1 RA–Zn(II) binding model.

and K_{app} is the apparent binding constant. For the system in TRIS buffer, the best fit yielded $K_{app} = 1.0 \pm 0.04 \times 10^4$ M^{-1} with $A_{max} = 0.46 \pm 0.01$, while in HEPES buffer the corresponding value was $K_{app} = 3.8 \pm 0.3 \times 10^3$ M^{-1} and $A_{max} = 0.43 \pm 0.02$ (Figure 2). Both fittings showed excellent correlation coefficients ($R^2 > 0.99$), confirming the adequacy of a simple 1:1 binding model.

The difference between the apparent binding constants obtained in TRIS and HEPES is best rationalized by pH, rather than intrinsic buffer effects. In fact, both TRIS and HEPES are zwitterionic good's buffers commonly used near physiological pH; however, TRIS can weakly coordinate Zn(II) through its amine group, potentially stabilizing labile metal species, whereas HEPES is largely noncoordinating and exerts minimal influence on Zn(II) speciation [45, 46]. In our experiments, the TRIS titration was conducted at pH 7.4, whereas the HEPES titration was at pH 7.2; under these conditions the UV–vis response was stronger in TRIS, consistent with a larger fraction of deprotonated catechol sites on RA available to chelate Zn(II). This pH-dependence was further confirmed by a control titration experiment in HEPES at pH 6.9, which produced much smaller spectral changes, indicating significantly weaker complex formation (Figure S3). Because catechol deprotonation shifts steeply across the neutral pH range, even a small ΔpH can substantially alter the concentration of the coordinating phenolate species, thereby increasing the effective binding constant and the intensity of the UV–vis response. Taken together, these observations show that pH is the dominant determinant of the Zn(II)–RA complex formation under our conditions, while TRIS and HEPES act as essentially comparable media when pH and ionic strength are matched. In contrast, when the titration was performed in phosphate buffer at the same pH, no appreciable spectral changes were detected upon Zn(II) addition. This behavior indicates that phosphate ions strongly compete with RA for Zn(II) coordination, thereby reducing the amount of free metal available to interact with the ligand. Consequently, the absence of detectable spectral variation in phosphate buffer supports the conclusion that Zn(II)–RA complex formation is highly sensitive to both pH and competing ligands present in solution, while the intrinsic effects of TRIS or HEPES are comparatively minor.

These results provided a reliable foundation for further NMR investigations of the Zn(II)-RA coordination mode in TRIS buffer. The metal titration obtained by acquiring ^{1}H 1D NMR spectra is shown in Figure 3. Progressive additions of Zn(II) induced pronounced changes in both chemical shift and line broadening of the aromatic proton signals associated with the caffeic acid moiety of RA, consistent with the formation of a coordination complex. Moreover, the two ethylenic protons were differently affected by the presence of the metal ion, with the proton at position 8 being the most significantly perturbed. These effects are consistent with those previously observed in phosphate buffer (Figure S1), although significantly more pronounced here, reinforcing the notion that phosphate ions compete with RA for Zn(II) binding and thereby attenuate the apparent coordination effects in phosphate medium.

From a structural perspective, the coordination of Zn(II) to RA is expected to involve the catechol hydroxyl groups of the caffeic acid moiety, which are preferred over those on the other aromatic ring. Although both rings contain vicinal hydroxyl groups, their acid–base and electronic properties differ markedly. This difference is evident from the NMR spectra of RA recorded as a function of pH (6.7–8.2), in which the protons of the caffeate portion display significant chemical shift variations, indicating a higher sensitivity of their local environment to pH changes—consistent with a lower pK_a and easier deprotonation (Figure 4). The investigated pH range was restricted by the chemical stability and solubility of RA. At alkaline pH values (around 9.0), RA undergoes rapid oxidation, generating multiple species in solution and preventing reliable NMR titration. Conversely, pH values below 6.7 could

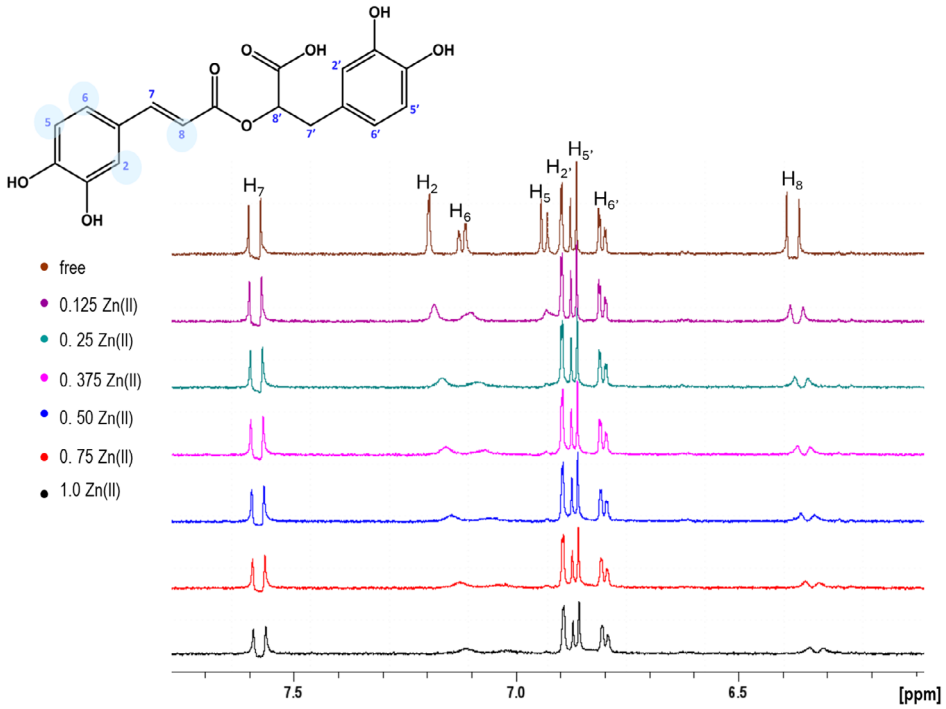

FIGURE 3 | ^{1}H NMR titration of RA with Zn(II) in 30 mM TRIS-d_{11} buffer at pH 7.4. Stacked ^{1}H NMR spectra (600 MHz, 298 K) of RA (500 μM) recorded upon incremental addition of $ZnCl_2$ (0–1.0 eqs). Progressive upfield shifts and line broadening are observed for the aromatic protons of the caffeic acid moiety, indicating direct involvement of this region in Zn(II) coordination.

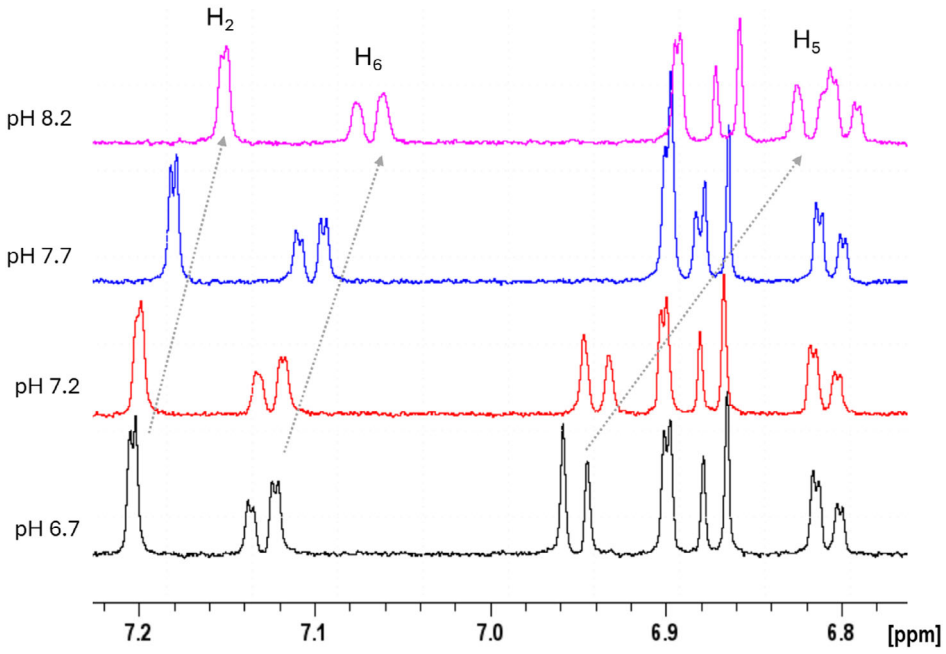

FIGURE 4 | Stacked ^{1}H NMR spectra (600 MHz, 298 K) of RA (500 μM) in water, 10% D_2O, recorded at different pH values.

not be explored due to the limited solubility of the ligand in aqueous medium. Taken together, these observations support a binding model in which Zn(II) preferentially interacts with the deprotonated catechol sites of the caffeic acid moiety of RA, forming a weak 1:1 complex whose stability is strongly affected by pH and buffer composition.

In addition to the observed chemical shift variations, the data in Figure 3 indicate that at Zn(II):RA ratios ≥ 0.75:1.0, the NMR resonances are substantially broadened and eventually become barely detectable. To gain further insight into the origin of this broadening, variable-temperature NMR experiments were performed. As shown in Figure S4, the line widths progressively decrease upon increasing the temperature, consistent with a shift toward a faster exchange regime. These observations suggest the presence of a dynamic equilibrium between the free and metal bound RA species undergoing exchange on an intermediate

NMR time scale. However, even at 313 K, further addition of Zn(II) beyond the 1:1 ratio leads to severe signal broadening and intensity loss, preventing a reliable estimation of the binding constant from NMR data (Figure S5). Similarly, previous studies combining NMR and mass spectrometry have also demonstrated chemical shift and line-broadening variations in the proton NMR signals of flavonoid molecules upon gradual addition of Zn(II), supporting a conserved binding mode with OH and carbonyl functional groups across different polyphenols [47].

The combined UV–vis and NMR evidence supports the formation of 1:1 RA–Zn(II) complex under physiological conditions, most likely involving coordination through the two catechol groups of the caffeate moiety. UV–vis titrations yielded a good fit to a 1:1 binding model, with an apparent binding constant log K ≈ 4 in TRIS buffer. Furthermore, in phosphate-containing buffers, Zn(II) can form Zn–phosphate complexes (log β_1 ≈ 2.7–3.5) [48], thereby limiting the Zn(II)–RA interaction. This competition likely reduces the concentration of free Zn(II) available for coordination with RA and may explain the absence of pronounced variations in both the NMR and UV–vis spectra recorded under these conditions.

On the other hand, the magnitude of the RA–Zn(II) affinity observed in TRIS is comparable to those reported for other catechol-containing natural polyphenols. For instance, caffeic acid and chlorogenic acid exhibit moderate Zn(II) binding with log K values typically in the 3–5 range, depending on pH and ionic strength [43, 49, 50]. Similarly, Zn(II) binds preferentially to the catechol moiety of rutin through adjacent phenolic oxygens on the 3′, 4′-dihydroxy B-ring, forming a distorted tetrahedral 1:1 complex. The apparent stability constant determined for this interaction was log K ≈ 3.2–3.5, under near-neutral pH conditions. DFT calculations confirmed that Zn(II) coordination occurs mainly via the catechol oxygens, with minor secondary stabilization from additional hydroxyl or glycosidic groups [49]. This coordination pattern and affinity closely mirror those observed for RA in the present study. Both ligands feature a catechol-containing subunit that provides two adjacent oxygen donors capable of chelating Zn(II). The binding constant determined for RA aligns well with the values reported for rutin, indicating that catechol-based polyphenols exhibit comparable Zn(II) affinities under physiological conditions. Overall, the RA comparison with related flavonoid complexes underscores a conserved coordination motif among natural catechol-containing polyphenols, where Zn(II) forms a reversible 1:1 chelate through adjacent hydroxyl donors [47]. The moderate stability constants reported for these systems point to a labile yet biologically relevant mode of interaction. Such complexes are sufficiently stable to transiently sequester Zn(II) and modulate its local availability, but not so strong as to prevent metal exchange or redistribution under physiological conditions. This balance between stability and lability is essential for maintaining metal homeostasis, allowing RA and similar polyphenols to act as dynamic regulators of Zn(II) speciation rather than as permanent chelators.

We next investigated the interaction between Zn(II) and the Aβ_{16} peptide under the same physiological conditions, using ^{1}H NMR spectroscopy to monitor the effects of metal coordination on the peptide's spectral features. Experiments were performed using a 0.5–0.6 mM solution of Aβ_{16} peptide with 0.3–1.5 equivalents of Zn(II), recorded at 288, 298, and 313 K at pH 7.4, using both phosphate and TRIS buffer. The temperature was lowered to 288 K to improve the detection of amide proton resonances, which are otherwise broadened beyond detection at higher temperatures due to exchange with water. In parallel, experiments at 313 K were conducted to compare the behavior of the system with that of the RA–Zn(II) complex previously described.

The choice of using the truncated Aβ_{16} peptide instead of the full-length Aβ_{40} or Aβ_{42} is justified by the fact that the N-terminal region, encompassing the first 16 residues, contains the primary metal-binding sites, including three histidine residues (His6, His13, and His14) that are known to coordinate metal ions such as zinc and copper [40–42, 51, 52]. The shorter Aβ_{16} fragment preserves the essential coordination motifs while offering significant advantages in terms of solubility, spectral resolution, and reduced aggregation propensity under experimental conditions. These factors make Aβ_{16} a suitable and widely accepted model for studying metal–peptide interactions at the molecular level, allowing for clearer interpretation of spectroscopic data without the complications introduced by the aggregation behavior of full-length Aβ peptides. NMR experiments performed on the apo peptide at 288 K revealed the presence of sequential Nuclear Overhauser Effect (NOE) connectivities between the amide protons of residues within the 9–12 region of the Aβ_{16} peptide. These dNN(i,i + 1) correlations are consistent with the formation of a turn motif, in line with previous structural observations reported for the apo form of Aβ_{16} [41, 52]. As previously reported, the addition of Zn(II) induces selective chemical-shift perturbations and significant line broadening in the NMR spectra, indicative of a dynamic equilibrium among multiple coordination species. The pronounced broadening observed at room temperature, which persists even upon increasing the Zn(II) concentration, points to an exchange process occurring in the intermediate regime on the NMR timescale and rules out a simple equilibrium between the free and fully bound forms. The metal-induced effects are most pronounced in the aromatic region, particularly at the resonances corresponding to the histidine residues, which are known primary metal-binding sites (Figure S6A). In addition, broadenings were also observed for residues located in proximity to the histidines, including Asp1, Glu11, Val12, Arg5, Asp7, and Gln15 (Figure S6B). These perturbations are in agreement with previous studies suggesting that Zn(II) may engage in coordination not only with histidine imidazole nitrogens but also with the carboxylate group of Glu11, Asp1 and Asp7 [53]. This coordination model may also account for the changes observed at Tyr10, possibly through local conformational effects or electrostatic perturbation due to proximity to the metal-binding site.

As expected, increasing the temperature improves the NMR signal quality and allows for a clearer monitoring of the chemical shift variations. The spectra recorded at 313 K show that Zn(II) addition induces to similar variations in the Aβ_{16} signals, with the largest effects observed for the aromatic resonances belonging to the three histidine residues, as well as those of Tyr10 and Phe4 (Figure S7). In addition, noticeable changes are detected for the methyl protons of Val12 and Ala2, and for the β- and γ-protons of Asp and Glu residues. Altogether, these observations reinforce the multifaceted nature of Zn(II) coordination in Aβ and support the existence of a heterogeneous ensemble of Aβ–Zn(II) species in solution, dynamically exchanging on the NMR timescale.

After evaluating the effect of Zn(II) alone on both the Aβ_{16} peptide and RA, we investigated the ternary system containing Aβ_{16},

Zn(II), and RA, the resulting ^{1}H NMR spectra were compared with those of the corresponding binary systems. The ternary system was analyzed using both phosphate and TRIS buffers, with NMR spectra recorded at three different temperatures: 288, 298, and 313 K. However, since phosphate was found to compete with RA for Zn(II) binding, we focused primarily on the analysis performed in TRIS buffer for the detailed investigations of the ternary system.

UV–vis spectra recorded for the ternary system indicate that RA is still able to bind Zn(II) in the presence of Aβ_{16}, as evidenced by the changes observed in the RA absorption bands upon metal addition (Figure 5). By comparing these spectra with those obtained for the RA–Zn(II) binary system, it is evident that the presence of Aβ_{16} significantly reduces the UV–vis absorption changes induced by equimolar Zn(II) amount. In fact, the variations observed are comparable to those recorded for the RA–Zn(II) system at a 1:0.3 RA:Zn ratio. This finding therefore supports the conclusion that, in the presence of Aβ_{16}, only about 30% of the RA in solution is coordinated to the metal ion. The 30% value can be rationalized by considering that the fraction of RA bound to Zn(II) corresponds to its involvement in the ternary Aβ_{16}–RA–Zn(II) system. In fact, if we take into account the apparent binding constants—approximately greater than 10^5 M^{-1} for Aβ_{16} [53] and 10^4 M^{-1} for RA—it becomes evident that Zn(II) has a much higher affinity for the peptide. Under equimolar conditions, this difference implies that the majority of the metal ions (more than 90–95%) are coordinated to Aβ_{16}, while only a small fraction remains associated with RA. Therefore, the observed 30% of RA affected by Zn(II) likely represents the portion engaged in ternary complex formation with Aβ and the metal ion.

While UV–vis spectroscopy clearly shows that RA remains coordinated to Zn(II) in the presence of Aβ_{16}, NMR analysis provides complementary insight into how the Aβ–Zn(II) system is affected by the presence of RA (Figure 6). Through NMR, it is possible to monitor the specific changes in the peptide resonances upon RA addition, offering a detailed view of how the ternary interaction modulates the metal coordination environment and the equilibrium among the different Aβ–Zn species. Analogously to what was observed for the Aβ_{16}–Zn(II) system, similar variations are detected upon addition of Zn(II) to the Aβ–RA mixture. The presence of RA does not initially induce any distinct changes in the proton resonances of Aβ_{16} upon progressive Zn(II) addition, as shown in Figure 7. This indicates that, at least in the early stages of titration, the coordination environment of Zn(II) around the peptide remains comparable in both systems.

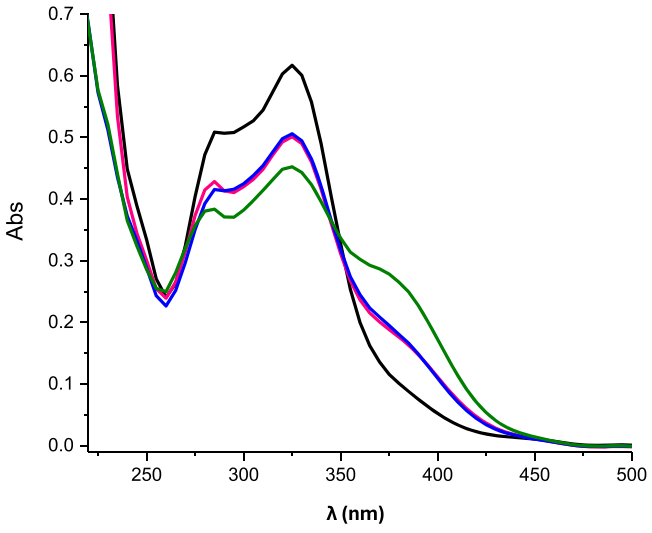

FIGURE 5 | UV–vis spectra of RA 50 μM + 50 μM Aβ_{16} (black), RA 50 μM + Aβ_{16} 50 μM + Zn(II) 50 μM (red), RA 50 μM + Zn(II) 15 μM (blue) and RA 50 μM + Zn(II) 50 μM (green). All the spectra were registered by preparing the solutions in TRIS 15 mM buffer at pH 7.5.

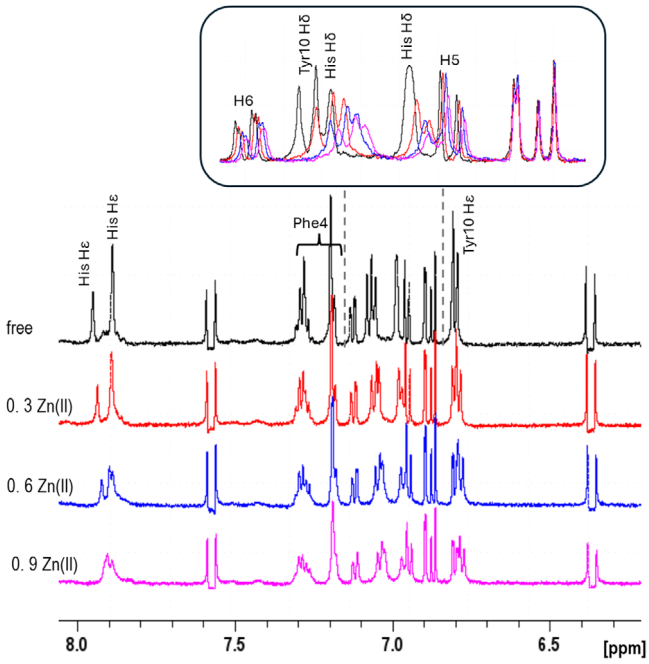

FIGURE 6 | ^{1}H NMR titration of Aβ_{16}-RA (1:1) mixture with Zn(II) in TRIS-d_{11} buffer at pH 7.4. Stacked ^{1}H NMR spectra (600 MHz, 313 K) of Aβ_{16} = RA = 500 μM recorded upon incremental addition of $ZnCl_2$ (0–0.9 eqs).

At the same time, slight variations are observed on the H5 and H6 resonances of RA (Figure 6), supporting the notion that the polyphenol also interacts with the metal ion. However, these changes are considerably smaller than those reported in Figure S5, suggesting that the majority of Zn(II) remains bound to the Aβ peptide. This is consistent with the expected difference in binding strength, as the apparent binding constant for the RA–Zn(II) complex is 1–2 orders of magnitude lower than that of the Zn(II)–Aβ system [53]. However, this observation appears to contrast with the UV–vis data, where the absorption changes recorded upon Zn(II) addition are still pronounced in the presence of the peptide. We also repeated the NMR measurements at a lower concentration, reducing it from 0.5 to 0.1 mM, thus approaching the concentration used in the UV–vis experiments (50 μM). However, the results remained unchanged, and the observed NMR effects were consistent at both concentrations (data not shown), thereby excluding concentration as a possible cause of the different behavior observed between the NMR and UV–vis experiments.

However, a more detailed analysis revealed that within ~2 min after the addition of 0.9 Zn(II) eqs to the Aβ–RA sample, a filamentous precipitate started to develop and continued to grow over time, gradually accumulating at the bottom of the NMR tube. Figure 8 shows the time-dependent overlays of the

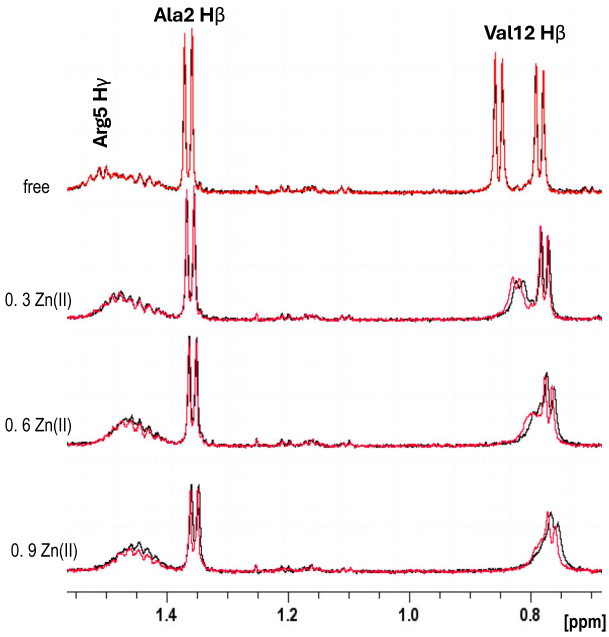

FIGURE 7 | Overlay of selected regions of the ^{1}H NMR spectra of Aβ_{16} in the absence (black) and presence (red) of an equimolar concentration of RA at different Zn(II): ligand ratios. Stacked ^{1}H NMR spectra (600 MHz, 313 K) of Aβ_{16} = RA = 500 μM in TRIS-d_{11} buffer (pH 7.4), recorded upon incremental addition of $ZnCl_2$ (0–0.9 eq).

aromatic region of the spectra, where progressive changes in the histidine resonances can be observed as the system undergoes precipitation. After 24 h a downfield shift is observed for both Aβ and RA protons that were initially the most affected by Zn(II) binding. Over time, a noticeable decrease in NMR signal intensity is also observed—∼50% for Aβ and 40% for RA—consistent with the gradual sample precipitation. Considering that neither RA nor Aβ alone forms a precipitate even upon Zn(II) additions exceeding a 1:1 ratio, it is reasonable to assume that the observed solid corresponds to the aggregation and precipitation of the ternary Aβ–Zn(II)–RA complex. Subsequently, the sample was centrifuged to separate the supernatant from the precipitate. The latter was then dissolved in DMSO-d_6, which—although not providing complete solubility—allowed sufficient dissolution to enable NMR spectral acquisition. Unfortunately, the spectra recorded in DMSO exhibited very broad and unresolved signals, preventing a detailed structural analysis of the systems (data not shown).

Taken together with the UV–vis and NMR data, these findings indicate that while Aβ dominates Zn(II) coordination, a fraction of the metal is also accessible to RA through secondary interactions that give rise to mixed Aβ–Zn(II)–RA adducts. In fact, although Zn(II) preferentially binds to Aβ, RA remains capable of coordinating the metal ion, likely establishing a dynamic equilibrium between Aβ-Zn(II) binary complex and Aβ-Zn(II)-RA ternary species in solution.

In order to obtain further evidence for the formation of the ternary adduct, NMR measurements were also carried out in phosphate buffer, which had previously been shown to compete with RA for Zn(II) binding. In phosphate buffer, the RA–Zn(II) complex exhibits selective, though very weak changes on the caffeate moiety; in the presence of Aβ_{16} these effects become broader (Figure S8). On the other hand, the peptide aromatic signals remain broadened both with and without RA, confirming that Aβ_{16} retains its Zn(II)-binding capacity. Finally, the subsequent analysis of the ^{1}H-^{1}H NOESY spectrum supported the occurrence of an interaction between RA and the Aβ_{16}–Zn(II) complex. In

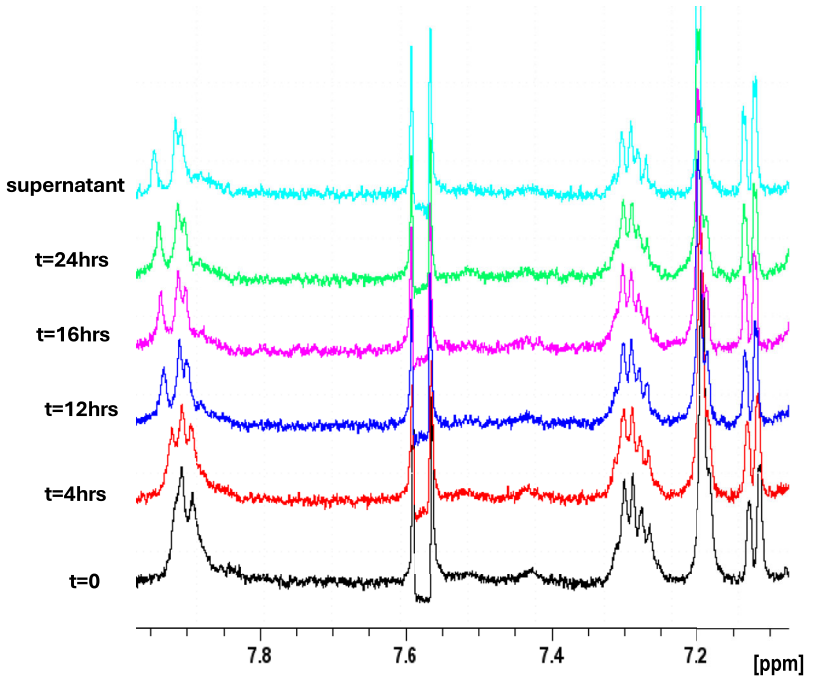

FIGURE 8 | Stacked ^{1}H NMR spectra (600 MHz, 313 K) of the Aβ_{16}–RA–Zn(II) system (Aβ_{16}= RA = 500 μM, $ZnCl_2$ = 0.9 eq) in TRIS-d_{11} buffer at pH 7.4, recorded as a function of time after Zn(II) addition. The aromatic region shows progressive changes consistent with the gradual formation and precipitation of the ternary Aβ–RA–Zn(II) complex. The final trace corresponds to the spectrum of the supernatant collected after centrifugation of the sample for 10 min.

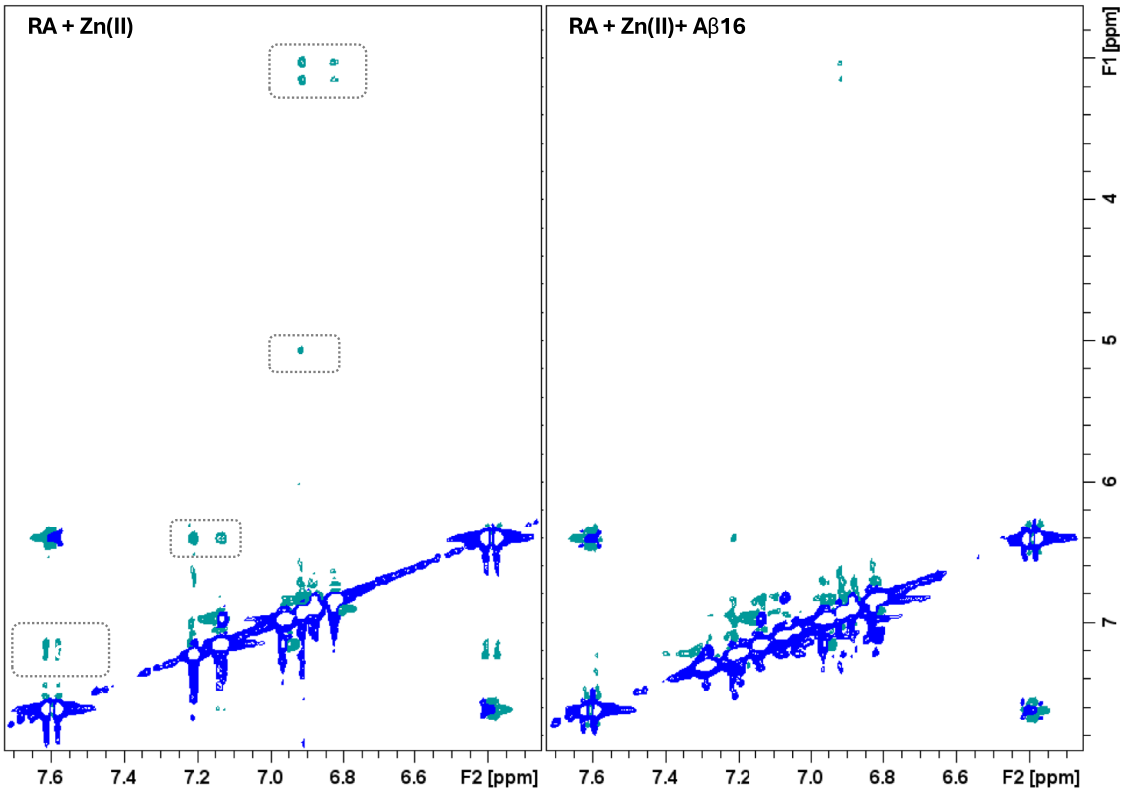

FIGURE 9 | Selected region of 2D ^{1}H-^{1}H NOESY spectra of RA-Zn(II) complex in absence (left) and in presence (right) of Aβ_{16}. Conditions: [RA] = [Aβ_{16}] = 0.5 mM, 20 mM phosphate buffer, pH 7.4, T = 298 K.

the RA + Zn(II) system, the small size and fast molecular tumbling of RA, results in weak, negative NOE cross-peaks between its aromatic and olefinic protons, as well as between the aromatic region and the aliphatic CH_2 and CH protons (Figure 9). However, in the presence of Aβ_{16} coordinated to Zn(II), these NOE signals are almost completely abolished. This behavior can be attributed to a change in the correlation time of RA upon binding to the peptide–metal complex. The interaction induces a slowing down of RA's molecular tumbling, shifting the NOE regime from negative (typical of fast-tumbling small molecules) toward positive values (typical of larger or transiently bound species). This leads to the disappearance of intraligand NOEs, strongly supporting RA ability to interact with the Aβ_{16}–Zn(II) complex in solution, resulting in altered motional and spatial relationships between its molecular domains.

To further investigate the possibility of a direct interaction between RA and histidine residues in the absence of metal ions, we also analyzed the chemical shift variations in the ^{1}H NMR spectra of the Aβ_{16} and Aβ_{12-16} peptides upon addition of RA under physiological conditions. Aβ_{16} contains three histidine residues (His6, His13, and His14), while Aβ_{12-16} includes only two (His13 and His14), allowing us to assess residue-specific contributions. In both cases, the addition of RA led to subtle yet reproducible chemical shift perturbations, particularly in the aromatic region associated with histidine side chains. These variations were modest in magnitude (<0.05 ppm), suggesting the presence of a weak, transient interaction rather than strong complex formation. The NMR data corresponding to the Aβ_{16} and RA system measured at T 288 K are shown in Figures 10 and 11, which illustrate (i) the minor yet consistent chemical shift changes observed on His aromatic protons upon RA addition (Figure 10) (ii) the slight perturbations on Aβ_{16} amide protons of Arg5, Asp7, Ser8, Glu11, Val12, and Gln15 as clearly indicated by overlapping the fingerprint regions of ^{1}H-^{1}H TOCSY recorded at T 288K (Figure 11) and (iii) the broadening of H2 and H6 proton of RA (Figure 10).

The extent of the perturbation was more pronounced in Aβ_{16}, indicating that His6 may contribute to the interaction interface. In Aβ_{12-16}, although the overall changes were less extensive, a similar trend was observed for His13 and His14, supporting the hypothesis of a general low-affinity association between RA and histidine residues (data not shown). The lack of significant signal broadening or NOE pattern changes further suggests that the interaction is not mediated by a conformational rearrangement or high-affinity binding, but likely arises from noncovalent contacts such as π–π stacking or hydrogen bonding between the phenolic rings of RA and the imidazole moieties of histidines. These findings indicate that RA can interact directly with histidine residues in amyloidogenic peptides, even in the absence of metal ions, though the interaction is weak and likely dynamic in nature.

Aβ-RA interactions have been previously observed by using different methods: (i) RA caused general chemical shift and broadening on NMR ^{1}H-^{15}N HSQC spectra of Aβ_{42} [54]; molecular docking and dynamics simulations revealed that RA binds with high affinity to the N-terminal region of Aβ, interacting with key residues such as His6, Tyr10, Glu11, Gly9, His13, His14, and Val12 through hydrogen bonding, π–π stacking, and van der Waals forces. These interactions destabilize the native conformation of Aβ, notably reducing its β-sheet content, and result in a

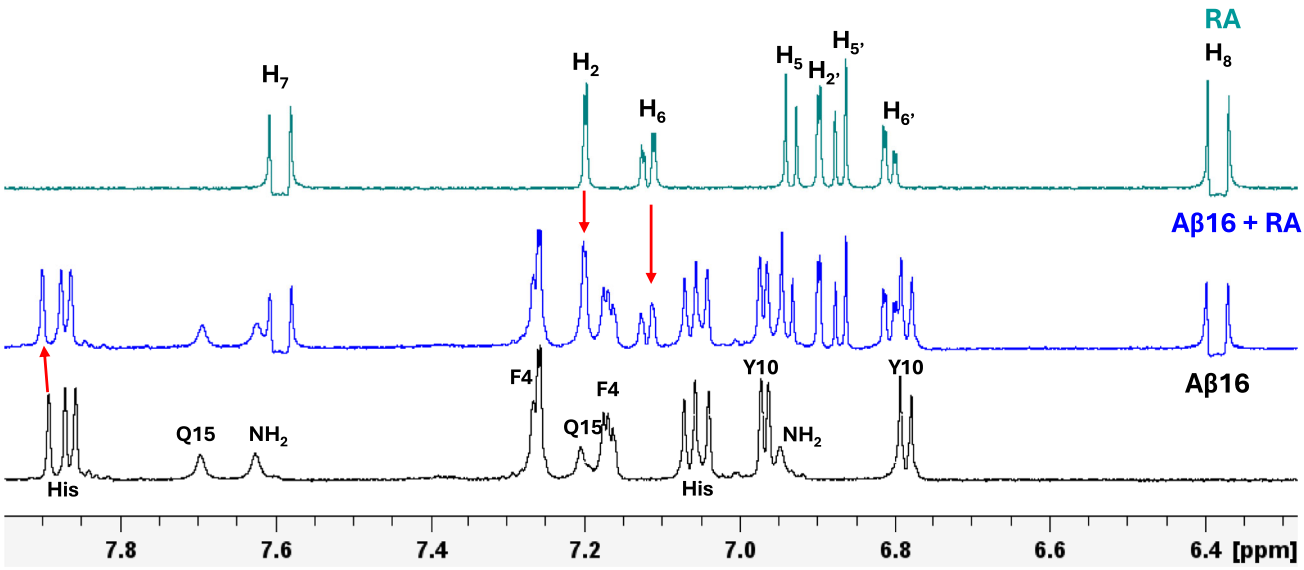

FIGURE 10 | Comparison of selected regions of 1D ^{1}H NMR spectra of (1) Aβ_{16} (black trace), (2) Aβ_{16} and RA $_{at}$ 1:1 stochiometric ratio (blue traces) and (3) RA. Conditions: [RA] = [Aβ_{16}] = 0.6 mM, 20 mM phosphate buffer, pH 7.4, T = 298 K.

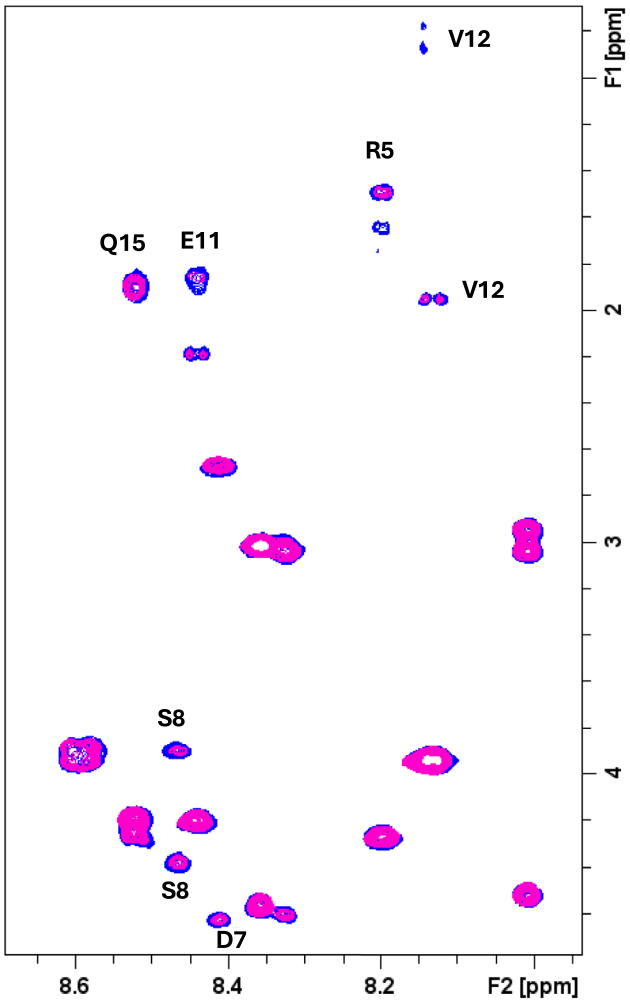

FIGURE 11 | Superimposition of 2D ^{1}H-^{1}H TOCSY spectra of Aβ_{16} (blue countours) in the absence and in the presence of 1.0 equivalents of RA (magenta countours). Conditions: [Aβ_{16}] = 0.6 mM, 20 mM phosphate buffer, pH 7.4, T = 288K.

negative binding free energy, indicating formation of a stable and inhibitory complex [55]; Replica Exchange Molecular Dynamics analysis identified six principal binding regions for RA and related polyphenols on the Aβ_{40} protofibril surface, notably including the disordered N-terminal tail accessible to ligand interaction [56].

At the same time, no significant chemical shift changes are observed for the protons of RA upon incubation with Aβ_{16} in the absence of Zn(II), although a slight line broadening is detected. This suggests the absence of strong, specific interactions between RA and the peptide under these conditions (Figure 10). Conversely, in the ternary Aβ_{16}–Zn(II)–RA system, the spectra reveal subtle but consistent chemical shift variations for RA signals (Figure 6) suggesting that RA interacts with Zn(II) in the presence of Aβ_{16} as well. The interaction between Aβ_{16} and RA appears to involve histidine residues, which simultaneously serve as anchoring points for Zn(II). Such behavior likely contributes to the formation of a ternary complex in which both Aβ_{16} and RA are coordinated to the metal ion. Moreover, the interaction between Aβ_{16} and RA is further stabilized upon Zn(II) binding, supporting the idea that the overall association is metal-mediated, with Zn(II) acting as a central coordination node that enhances the affinity between the peptide and RA. Similar behavior was observed with the Aβ_{16}–Cu(II)–RA system, where Cu(II)-RA association was stabilized in the presence of Aβ_{16}, as indicated by the induced paramagnetic line broadening on protons signals of RA [5]. RA in the cupric ternary adduct demonstrated the ability to scavenge ROS generated by the Aβ_{16}–Cu(II) complex, both in its pure form and when present within the rosemary extract [11]. Notably, the extract exhibited a greater protective effect compared to the isolated compound.

Our findings support the ability of RA to bind Zn(II) both in presence and in absence of Aβ. Zinc ions have been widely recognized as key modulators of Aβ peptide aggregation, primarily through their ability to coordinate with histidine (His6, His13, and His14) located in the N-terminal region of the peptide. Notably, upon

addition of Zn(II) to the Aβ–RA mixture, a filamentous precipitate gradually formed and accumulated over time, indicating a substantial change in the physicochemical properties of the ternary system compared to the Aβ–Zn(II) binary complex. This phenomenon suggests that RA might interfere with the aggregation dynamics of Aβ, possibly by modulating metal-mediated cross-linking and leading to the formation of species with altered solubility or morphology. Such behavior aligns with the dual role of natural polyphenols like RA, which have gained attention as multitarget agents due to their combined metal-chelating capacity and antiamyloidogenic effects. Although relatively weak, the interaction of RA with the Aβ–Zn(II) complex may attenuate Zn-induced aggregation and favor the stabilization of less toxic peptide conformations. This interpretation is consistent with the observed precipitation process and supported by preliminary data on the coordination chemistry between RA, Zn(II), and the N-terminal fragment of Aβ. Further studies involving more aggregation-prone peptide sequences, such as Aβ_{40}, Aβ_{42}, or protofibrillar models, will be necessary to determine whether RA–Zn(II) coordination can effectively prevent aggregate nucleation, inhibit fibril elongation, or promote the disassembly of preformed aggregates.

Moreover, translating these coordination insights into a physiological context necessitates an evaluation of RA's ability to cross the blood–brain barrier (BBB). RA exhibits physicochemical properties that generally support oral absorption, fully complying with Lipinski's rule of five. Nevertheless, despite this favorable drug-like profile, its actual intestinal absorption is remarkably low, with estimates around 1% of the administered dose, largely due to limited epithelial permeability and extensive presystemic metabolism by gut microflora and enzymes. Furthermore, data indicate that the BBB effectively prevents RA from penetrating into the central nervous system, thus severely limiting its distribution to the brain after systemic administration. Experimental studies detected only trace amounts of RA in brain tissue, confirming its naturally low BBB permeability [57]. At the same time, nanocarrier-based delivery systems have shown promising results in enhancing RA brain uptake [58–61], for example intranasal administration of RA-loaded solid lipid nanoparticles achieved a mouse brain concentration of 5.69 μg within 1 h, with pharmacokinetic parameters indicating effective systemic absorption [61]. This nose-to-brain delivery approach successfully bypasses the BBB, enhancing cerebral uptake of RA and limiting systemic exposure, highlighting the importance of designing optimized delivery platforms for future in vivo studies.

3 | Conclusion

This work elucidates the coordination behavior of RA toward Zn(II) under near-physiological conditions through a combined UV–vis and NMR approach. The spectroscopic data demonstrate the formation of a 1:1 RA–Zn(II) complex involving the deprotonated catechol groups of the caffeic acid moiety. The binding strength (log K ≈ 4) and its pronounced dependence on pH and buffer composition reflect a labile, pH-sensitive coordination mode typical of catechol-based ligands. Competition experiments in phosphate buffer further highlight the role of medium composition, as Zn–phosphate complexation effectively suppresses RA binding.

The moderate stability of the RA–Zn(II) complex supports a dynamic coordination behavior consistent with biological metal homeostasis, where transient interactions regulate local Zn(II) speciation rather than permanently chelating the ion. In the presence of Aβ, Zn(II) coordination is largely peptide-driven, yet a fraction of the metal remains accessible to RA, giving rise to mixed Aβ–Zn(II)–RA adducts. The appearance of a filamentous precipitate upon Zn(II) addition indicates a distinct alteration in the physicochemical properties of the ternary system, suggesting that RA may influence metal-mediated aggregation equilibria through secondary coordination.

These results provide a bioinorganic framework for understanding how natural catecholic polyphenols interact with Zn(II) under physiological conditions and in the presence of competing biomolecular ligands. Beyond their chemical significance, these findings underscore the importance of targeting metal–peptide complexes in Alzheimer's disease as a complementary strategy to conventional approaches focused solely on amyloid clearance. Future investigations employing more physiologically relevant amyloidogenic systems (Aβ_{40}, Aβ_{42}, or protofibrillar models), coupled with in vivo studies utilizing validated delivery platforms, will be essential to assess whether RA–Zn(II) coordination can modulate aggregation pathways in a biological context.

To date, no studies have directly examined rosmarinic acid within the brain environment, largely due to the limited permeability of the BBB and the absence of targeted delivery strategies in humans. Addressing this gap will be crucial to determine whether the coordination chemistry elucidated here can translate into a tangible therapeutic effect. With continued advances in nanocarrier and brain-targeted delivery technologies, it may eventually become possible to transport RA effectively into the central nervous system—unlocking new opportunities for the rational design of bioinspired, multitarget agents capable of modulating metal homeostasis and amyloid aggregation in neurodegenerative disease.

4 | Experimental Section

4.1 | Materials

$Zn(ClO_4)_2$, rosmarinic acid (≥98.0% HPLC), TMSP-d_4 (3-(trimethylsilyl)-[2,2,3,3-d_4] propane-1-sulfonate sodium salt, HEPES (4-(2-hydroxyethyl)-1-piperazineethanesulfonic acid), TRIS (tris (hydroxymethyl)aminomethane)), TRIS-d_{11} 1 M solution, phosphate buffer 1 M solution, DMSO-d_6, and D_2O were all supplied by Sigma–Aldrich (Schnelldorf, Germany). The Aβ_{16} peptide was purchased from DBA Italia (Segrate, Italy).

4.2 | NMR Measurements

NMR samples were prepared in HPLC-grade distilled water containing 10% D_2O and TMSP-d_4 as internal chemical shift reference. Physiological pH was maintained by dissolving rosmarinic acid and Aβ_{16} peptide in a 15–30 mM buffer solution. The desired concentration of Zn(II) ions in each NMR tube was achieved by adding small aliquots of concentrated aqueous Zn(II) stock solutions.

All NMR experiments were conducted on a Bruker Avance III 600 MHz spectrometer, with temperature control maintained

within ±0.2 K. Measurements were performed at 313, 298, and 288 K, depending on the experimental conditions and proton exchange considerations. A 5 mm broadband inverse (BBI) probe was employed for acquisition. Suppression of the residual water signal was achieved through the excitation sculpting method, using a 2 ms selective square pulse centered on the water resonance [52]. Standard ^{1}H spectra were acquired with 16 transients, a spectral width of 7200 Hz, and a recycle delay of 2.0 s. Proton resonance assignments of the ligand were determined through a combination of 1D and 2D NMR experiments, including TOCSY and NOESY. TOCSY spectra were obtained using the MLEV-17 sequence with a spin-lock mixing time of 60 ms, while NOESY experiments were recorded with variable mixing times to optimize cross-relaxation detection. All spectral data were processed and analyzed using TopSpin 3.6 software (Bruker BioSpin).

4.3 | UV–vis Measurements

The analyzed samples were prepared using a final concentration of RA of 5.0×10^{-5} M in the cuvette, obtained by diluting stock solutions with either buffers or HPLC-grade distilled water. Zinc titration was performed using a stock solution of $Zn(ClO_4)_2$ in HPLC-grade water. The absorption spectra were recorded on an Agilent Cary 60 UV–vis spectrophotometer, using a Hellma Analytics high-precision quartz Suprasil cell. Spectra were collected at room temperature over the range of 200–800 nm and subsequently processed using OriginPro 8.5 software.

Acknowledgements

The MUR-PRIN 2022 grant number 2022RCRWE5 and the Consorzio Interuniversitario Risonanze Magnetiche di Metallo Proteine (CIRMMP) are acknowledged for the support.

Open access publishing facilitated by Universita degli Studi di Siena, as part of the Wiley - CRUI-CARE agreement.

Funding

This work was supported by MUR-PRIN 2022 (Grant 2022RCRWE5).

Conflicts of Interest

The authors declare no conflicts of interest.

Data Availability Statement

The data that support the findings of this study are available from the corresponding author upon reasonable request.

References

1. P. Velander, L. Wu, S. B. Hildreth, et al., "Catechol-Containing Compounds Are a Broad Class of Protein Aggregation Inhibitors: Redox State Is a Key Determinant of the Inhibitory Activities," *Pharmacological Research* 184 (2022): 106409.

2. M. Sekiguchi, M. Horiuchi, A. Tanaka, et al., "Inhibitory Activity of Amyloid-β Aggregation by Flavonoids and Rosmarinic Acid Related Compounds Isolated from Zostera Marina," *Bioscience, Biotechnology, and Biochemistry* 89 (2025): 941–944.

3. R. H. Khan, M. K. Siddiqi, V. N. Uversky, and P. Salahuddin, "Molecular Docking of Aβ1-40 Peptide and Its Iowa D23N Mutant Using Small Molecule Inhibitors: Possible Mechanisms of Aβ-Peptide Inhibition," *International Journal of Biological Macromolecules* 127 (2019): 250–270.

4. M. Yamada, K. Ono, T. Hamaguchi, and M. Noguchi-Shinohara, Natural Compounds as Therapeutic Agents for Amyloidogenic Diseases, ed. N. Vassallo (Springer International Publishing, 2015), 79–94.

5. A. Kola, A. Hecel, S. Lamponi, and D. Valensin, "Novel Perspective on Alzheimer's Disease Treatment: Rosmarinic Acid Molecular Interplay with Copper(II) and Amyloid β," *Life* 10 (2020): 118.

6. P. B. Kasi, K. Molnár, L. László, and M. Kotormán, "Peppermint Extract Inhibits Protein Aggregation," *Biologia Futura* 72 (2021): 367–372.

7. R. Ştefănescu, "Quantification of Amyloid-β Aggregation Inhibitors Gallic Acid and Rosmarinic Acid in Biological Samples by LC-MS/MS," *Analytical Biochemistry* 700 (2025): 115799.

8. K. Ogawa, A. Ishii, A. Shindo, et al., "Spearmint Extract Containing Rosmarinic Acid Suppresses Amyloid Fibril Formation of Proteins Associated with Dementia," *Nutrients* 12 (2020): 3480.

9. R. Taguchi, K. Hatayama, T. Takahashi, et al., "Structure–activity Relations of Rosmarinic Acid Derivatives for the Amyloid β Aggregation Inhibition and Antioxidant Properties," *European Journal of Medicinal Chemistry* 138 (2017): 1066–1075.

10. D. M. Hanafy, G. E. Burrows, P. D. Prenzler, and R. A. Hill, "Potential Role of Phenolic Extracts of Mentha in Managing Oxidative Stress and Alzheimer's Disease," *Antioxidants* 9 (2020): 631.

11. A. Kola, G. Vigni, S. Lamponi, and D. Valensin, "Protective Contribution of Rosmarinic Acid in Rosemary Extract Against Copper-Induced Oxidative Stress," *Antioxidants* 13 (2024): 1419.

12. N. A. Kelsey, H. M. Wilkins, and D. A. Linseman, "Nutraceutical Antioxidants as Novel Neuroprotective Agents," *Molecules* 15 (2010): 7792–7814.

13. F. N. S. Fachel, R. S. Schuh, K. S. Veras, et al., "An Overview of the Neuroprotective Potential of Rosmarinic Acid and Its Association with Nanotechnology-Based Delivery Systems: A Novel Approach to Treating Neurodegenerative Disorders," *Neurochemistry International* 122 (2019): 47–58.

14. E. P. de Lima, L. F. Laurindo, V. C. S. Catharin, et al., "Polyphenols, Alkaloids, and Terpenoids Against Neurodegeneration: Evaluating the Neuroprotective Effects of Phytocompounds Through a Comprehensive Review of the Current Evidence," *Metabolites* 15 (2025): 124.

15. X. Han, B. Han, Y. Zhao, et al., "Rosmarinic Acid Attenuates Rotenone-Induced Neurotoxicity in SH-SY5Y Parkinson's Disease Cell Model through Abl Inhibition," *Nutrients* 14 (2022): 3508.

16. F. J. Mirza and S. Zahid, "Ursolic Acid and Rosmarinic Acid Ameliorate Alterations in Hippocampal Neurogenesis and Social Memory Induced by Amyloid Beta in Mouse Model of Alzheimer's Disease," *Frontiers in Pharmacology* 13 (2022): 1058358.

17. J. Lakey-Beitia, A. M. Burillo, G. La Penna, M. L. Hegde, and K. S. Rao, "Polyphenols as Potential Metal Chelation Compounds Against Alzheimer's Disease," *Journal of Alzheimer's Disease* 82 (2021): S335–S357.

18. A. Kola, D. Dudek, and D. Valensin, "Metal Complexation Mechanisms of Polyphenols Associated to Alzheimer's Disease," *Current Medicinal Chemistry* 28 (2021): 7278–7294.

19. C. Luo, L. Zou, H. Sun, et al., "A Review of the Anti-Inflammatory Effects of Rosmarinic Acid on Inflammatory Diseases," *Frontiers in Pharmacology* 11 (2020): 153.

20. P. K. Walencik, R. Choińska, E. Gołębiewska, and M. Kalinowska, "Metal–Flavonoid Interactions—From Simple Complexes to Advanced Systems," *Molecules* 29 (2024): 2573.

21. A. M. Khvan, E. L. Kristallovich, and K. A. Abduazimov, "Complexation of Caffeic and Ferulic Acids by Transition-Metal Ions," *Chemistry of Natural Compounds* 37 (2001): 72–75.

22. C. Maerten, L. Lopez, P. Lupattelli, et al., "Electrotriggered Confined Self-Assembly of Metal–Polyphenol Nanocoatings Using a Morphogenic Approach," *Chemistry of Materials* 29 (2017): 9668–9679.

23. D. Tomasetig, C. Wang, N. Hondl, A. Friedl, and H. Ejima, "Exploring Caffeic Acid and Lignosulfonate as Key Phenolic Ligands for Metal-Phenolic Network Assembly," *ACS Omega* 9 (2024): 20444–20453.

24. Y. O. Ayipo, W. A. Osunniran, H. F. Babamale, M. O. Ayinde, and M. N. Mordi, "Metalloenzyme Mimicry and Modulation Strategies to Conquer Antimicrobial Resistance: Metal-Ligand Coordination Perspectives," *Coordination Chemistry Reviews* 453 (2022): 214317.

25. G. Mazzone, "On the Inhibition of Hydroxyl Radical Formation by Hydroxycinnamic Acids: The Case of Caffeic Acid as a Promising Chelating Ligand of a Ferrous Ion," *The Journal of Physical Chemistry. A* 123 (2019): 9560–9566.

26. P. W. Linder and A. Voyé, "Potentiometric Investigations of the Equilibria between Caffeic Acid and Copper(II), Zinc(II), Iron(II) and Hydrogen Ions in Aqueous Solution," *Polyhedron* 6 (1987): 53–60.

27. U. C. Müller, T. Deller, and M. Korte, "Not Just Amyloid: Physiological Functions of the Amyloid Precursor Protein Family," *Nature Reviews Neuroscience* 18 (2017): 281–298.

28. X. Sun, W.-D. Chen, and Y.-D. Wang, "β-Amyloid: The Key Peptide in the Pathogenesis of Alzheimer's Disease," *Frontiers in Pharmacology* 6 (2015): 221.

29. L. Wang, Y.-L. Yin, X.-Z. Liu, et al., "Current Understanding of Metal Ions in the Pathogenesis of Alzheimer's Disease," *Translational Neurodegeneration* 9 (2020): 10.

30. Y. Liu, M. Nguyen, A. Robert, and B. Meunier, "Metal Ions in Alzheimer's Disease: A Key Role or Not?" *Accounts of Chemical Research* 52 (2019): 2026–2035.

31. L.-L. Chen, Y.-G. Fan, L.-X. Zhao, Q. Zhang, and Z.-Y. Wang, "The Metal Ion Hypothesis of Alzheimer's Disease and the Anti-Neuroinflammatory Effect of Metal Chelators," *Bioorganic Chemistry* 131 (2023): 106301.

32. L. Mezzaroba, D. F. Alfieri, A. N. Colado Simão, and E. M. Vissoci Reiche, "The Role of Zinc, Copper, Manganese and Iron in Neurodegenerative Diseases," *NeuroToxicology* 74 (2019): 230–241.

33. A. Abelein, A. Gräslund, and J. Danielsson, "Zinc as Chaperone-Mimicking Agent for Retardation of Amyloid β Peptide Fibril Formation," *Proceedings of the National Academy of Sciences* 112 (2015): 5407–5412.

34. M. C. McCord and E. Aizenman, "The Role of Intracellular Zinc Release in Aging, Oxidative Stress, and Alzheimer's Disease," *Frontiers in Aging Neuroscience* 6 (2014): 77.

35. Y. Yuan, F. Niu, Y. Liu, and N. Lu, "Zinc and Its Effects on Oxidative Stress in Alzheimer's Disease," *Neurological Sciences* 35 (2014): 923–928.

36. C. Cheignon, M. Tomas, D. Bonnefont-Rousselot, P. Faller, C. Hureau, and F. Collin, "Oxidative Stress and the Amyloid Beta Peptide in Alzheimer's Disease," *Redox Biology* 14 (2018): 450–464.

37. E. Gaggelli, H. Kozlowski, D. Valensin, and G. Valensin, "Copper Homeostasis and Neurodegenerative Disorders (Alzheimer's, Prion, and Parkinson's Diseases and Amyotrophic Lateral Sclerosis," *Chemical Reviews* 106 (2006): 1995–2044.

38. M. A. Greenough, J. Camakaris, and A. I. Bush, "Metal Dyshomeostasis and Oxidative Stress in Alzheimer's Disease," *Neurochemistry International* 62 (2013): 540–555.

39. H. Kozlowski, M. Luczkowski, M. Remelli, and D. Valensin, "Copper, Zinc and Iron in Neurodegenerative Diseases (Alzheimer's, Parkinson's and Prion Diseases)," *Coordination Chemistry Reviews* 256 (2012): 2129–2141.

40. C. Migliorini, E. Porciatti, M. Luczkowski, and D. Valensin, "Structural Characterization of Cu^{2+}, Ni^{2+} and Zn^{2+} Binding Sites of Model Peptides Associated with Neurodegenerative Diseases," *Coordination Chemistry Reviews* 256 (2012): 352–368.

41. V. Minicozzi, F. Stellato, M. Comai, et al., "Identifying the Minimal Copper- and Zinc-Binding Site Sequence in Amyloid-β Peptides*," *Journal of Biological Chemistry* 283 (2008): 10784–10792.

42. P. Faller, "Copper and Zinc Binding to Amyloid-β: Coordination, Dynamics, Aggregation, Reactivity and Metal-Ion Transfer," *Chembiochem* 10 (2009): 2837–2845.

43. M. Kalinowska, J. Sienkiewicz-Gromiuk, G. Świderski, A. Pietryczuk, A. Cudowski, and W. Lewandowski, "Zn(II) Complex of Plant Phenolic Chlorogenic Acid: Antioxidant, Antimicrobial and Structural Studies," *Materials* 13 (2020): 3745.

44. A. Kola, G. Vigni, M. C. Baratto, and D. Valensin, "A Combined NMR and UV–Vis Approach to Evaluate Radical Scavenging Activity of Rosmarinic Acid and Other Polyphenols," *Molecules* 28 (2023): 6629.

45. C. M. H. Ferreira, I. S. S. Pinto, E. V. Soares, and H. M. V. M. Soares, "(Un)suitability of the use of pH Buffers in Biological, Biochemical and Environmental Studies and Their Interaction with Metal Ions – a Review," *Rsc Advances* 5 (2015): 30989–31003.

46. D. Wyrzykowski, A. Tesmar, D. Jacewicz, J. Pranczk, and L. Chmurzyński, "Zinc(II) Complexation by Some Biologically Relevant pH Buffers," *Journal of Molecular Recognition* 27 (2014): 722–726.

47. Y. Wei and M. Guo, "Zinc-Binding Sites on Selected Flavonoids," *Biological Trace Element Research* 161 (2014): 223–230.

48. K. J. Powell, P. L. Brown, R. H. Byrne, et al., "Chemical Speciation of Environmentally Significant Metals with Inorganic Ligands. Part 5: The Zn^{2+} + OH^-, Cl^-, CO_3^{2-}, SO_4^{2-}, and PO_4^{3-} Systems (IUPAC Technical Report," *Pure and Applied Chemistry* 85 (2013): 2249–2311.

49. H. C. Da Silva, L. A. De Souza, H. F. Dos Santos, and W. B. De Almeida, "Determination of Anticancer Zn(II)–Rutin Complex Structures in Solution through Density Functional Theory Calculations of 1H NMR and UV–VIS Spectra," *ACS Omega* 5 (2020): 3030–3042.

50. J. Gao, F. Xing, Y. Bai, and S. Zhu, "Synthesis, Spectroscopy, and Binding Constants of Ketocatechol-Containing Iminodiacetic Acid and Its Fe(III), Cu(II), and Zn(II) Complexes and Reaction of Cu(II) Complex with H2O2 in Aqueous Solution," *Dalton Transactions* 43 (2014): 7964–7978.

51. Á. Grenács and I. Sóvágó, "Copper(II), Nickel(II) and Zinc(II) Complexes of the N-Terminal Nonapeptide Fragment of Amyloid-β and Its Derivatives," *Journal of Inorganic Biochemistry* 139 (2014): 49–56.

52. G. De Gregorio, F. Biasotto, A. Hecel, M. Luczkowski, H. Kozlowski, and D. Valensin, "Structural Analysis of Copper(I) Interaction with Amyloid β Peptide," *Journal of Inorganic Biochemistry* 195 (2019): 31–38.

53. B. Alies, A. Conte-Daban, S. Sayen, et al., "Zinc(II) Binding Site to the Amyloid-β Peptide: Insights from Spectroscopic Studies with a Wide Series of Modified Peptides," *Inorganic Chemistry* 55 (2016): 10499–10509.

54. N. Iwaya, N. Goda, M. Matsuzaki, et al., "Principal Component Analysis of Data from NMR Titration Experiment of Uniformly 15N Labeled Amyloid Beta (1–42) Peptide with Osmolytes and Phenolic Compounds," *Archives of Biochemistry and Biophysics* 690 (2020): 108446.

55. L. Zhao, W. Jiang, Z. Zhu, et al., "Rosemarinic Acid-Induced Destabilization of Aβ Peptides: Insights from Molecular Dynamics Simulations," *Foods* 13 (2024): 4170.

56. F. Tavanti, A. Pedone, and M. C. Menziani, "Computational Insight into the Effect of Natural Compounds on the Destabilization of Preformed Amyloid-β(1–40) Fibrils," *Molecules* 23 (2018): 1320.

57. M. Hitl, N. Kladar, N. Gavarić, and B. Božin, "Rosmarinic Acid–Human Pharmacokinetics and Health Benefits," *Planta Medica* 87 (2021): 273–282.

58. C. Jia, Y. Gou, Y. Gao, et al., "Rosmarinic Acid Liposomes Suppress Ferroptosis in Ischemic Brain via Inhibition of TfR1 in BMECs," *Phytomedicine* 132 (2024): 155835.

59. A. Stasiłowicz-Krzemień, N. Rosiak, A. Płazińska, et al., "Cyclodextrin Derivatives as Promising Solubilizers to Enhance the Biological Activity of Rosmarinic Acid," *Pharmaceutics* 14 (2022): 2098.

60. Y.-C. Kuo and R. Rajesh, "Targeted Delivery of Rosmarinic Acid across the Blood–brain Barrier for Neuronal Rescue Using Polyacrylamide-Chitosan-Poly(lactide-*co*-Glycolide) Nanoparticles with Surface Cross-Reacting material 197 and Apolipoprotein E," *International Journal of Pharmaceutics* 528 (2017): 228–241.

61. R. Bhatt, D. Singh, A. Prakash, and N. Mishra, "Development, Characterization and Nasal Delivery of Rosmarinic Acid-Loaded Solid Lipid Nanoparticles for the Effective Management of Huntington's Disease," *Drug Delivery* 22 (2015): 931–939.

Supporting Information

Additional supporting information can be found online in the Supporting Information Section. **Supporting Fig. S1:** Selected regions of the ^{1}H NMR spectra of RA recorded in the absence (black trace) and in the presence of increasing amounts of Zn(II) (0.125-0.75 eqs.; colored traces). The chemical structure along with proton numbering is shown. Conditions: [RA] = 0.5 mM, 20 mM phosphate buffer, pH 7.4, T = 298 K. **Supporting Fig. S2:** Selected region of UV-VIS spectrum of RA 50μM in absence (black) and in the presence of increasing Zn(II) ratios (0.1 red; 0.2 green; 0.3 blue; 0.4 cyan; 0.5 magenta; 0.6 yellow, 0.7 olive; 0.8 dark blue; 0.9 purple; 1.0 brown). **Supporting Fig. S3:** UV-VIS spectra of RA 50μM in absence and in the presence of increasing Zn(II) ratios (from 0.1 to 10) in HEPES 15 mM, pH 6.9. **Supporting Fig. S4:** Selected regions of the 1H NMR spectra of RA in the presence of 1.0 Zn(II) eqs. recorded at different temperatures. Conditions: [RA] = 0.5 mM, 30 mM TRIS, pH 7.4. **Supporting Fig. S5:** Stacked ^{1}H NMR spectra (600 MHz, 313 K) of rosmarinic acid (RA, 0.5 mM) in TRIS-d_{11} buffer at pH 7.4, recorded upon incremental addition of $ZnCl_2$. The black spectrum corresponds to free RA, while the colored spectra (from bottom to top) represent increasing Zn(II) equivalents: 0.3, 0.6, 0.75, 0.9, 1.5, 2.0, and 3.0 eq. **Supporting Fig. S6:** Overlay of the 1D ^{1}H spectrum (A) and the 2D ^{1}H–^{1}H TOCSY spectrum (B) of $A\beta_{16}$ recorded in the absence (black) and in the presence of 0.75 equivalents of Zn(II) (magenta/blue). Assigned resonances affected by metal addition are indicated. Experimental conditions: [$A\beta_{16}$] = 0.50 mM, 20 mM phosphate buffer, pH 7.4, 298 K. **Supporting Fig. S7:** Stacked ^{1}H NMR spectra (600 MHz, 313 K) of $A\beta_{16}$ 0.5 mM in TRIS-d_{11} buffer at pH 7.4, recorded upon incremental addition of $ZnCl_2$. The black spectrum corresponds to free $A\beta_{16}$, while the colored spectra represent increasing Zn(II) equivalents: 0.3, 0.6 and 0.9 eq. **Supporting Fig. S8:** Superimposition of 1D ^{1}H NMR spectra of RA- $A\beta_{16}$ mixture at 1:1 ratio recorded in the absence of metal ions (black trace), in the presence of 0.5 (red), 1.0 (blue) and 1.5 (magenta) equivalents of Zn(II). Conditions: [RA] = 0.5 mM, 20 mM phosphate buffer, pH 7.4, T = 298 K.